AAS 21-234

# EXPLORATION OF DEIMOS AND PHOBOS LEVERAGING RESONANT ORBITS

David Canales*, Maaninee Gupta†, Beom Park‡, and Kathleen C. Howell§

While the interest in future missions devoted to Phobos and Deimos increases, missions that explore both moons are expensive in terms of maneuver capabilities partly due to low-energy transfer options that may not be readily available. The proposed approach in this investigation includes Mars-Deimos resonant orbits that offer repeated Deimos flybys as well as access to libration point orbits in the Phobos vicinity. A strategy to select the candidate orbits is discussed and associated costs are analyzed, both for impulsive and low-thrust propulsion capabilities, within the context of the coupled spatial circular restricted three body problem. The trajectory concepts are then validated in a higher-fidelity ephemeris model.

## INTRODUCTION

The future of space exploration includes a focus on Mars and its moons, Phobos and Deimos. Although not generally a primary objective, observations of these two moons as part of various Mars missions have occurred since the 1990's.[1] One example is the Phobos 2 mission,[1] where contact was lost when the spacecraft was approaching the surface of Phobos. However, both moons are now considered potentially key destinations in support of the Martian exploration program including, for example, telecommunications capabilities, radiation protection, and infrastructure for transportation and operations.[2,3] Recognizing the importance of both moons, a number of missions to explore Phobos and Deimos have been proposed by both ESA and NASA, including PHOOTPRINT,[4] PANDORA,[5] and PADME.[6] In addition, JAXA's MMX,[7] planned for launch in 2024, incorporates the return of a sample from Phobos to Earth.[8] While some of the proposed mission scenarios are based on different scientific objectives, many are focused on exploring only one of the two moons.

Given the small masses of both Martian moons, constructing low-propellant transfers is challenging, particularly for capture into a science orbit in the vicinity of either of the two moons. In contrast to other multi-moon planetary systems such as Jupiter or Uranus, the gravitational influence of the Martian moons is so small that the moons do not significantly influence the path of a spacecraft (s/c) when traversing the Martian vicinity. Consequently, capture at either moon is challenging using the classical two-body problem (2BP). With the objective of performing in-situ observation of Phobos, previous authors have proposed different alternatives based on Lambert arcs to arrive at Phobos and

*Ph.D. Candidate, School of Aeronautics and Astronautics, Purdue University, West Lafayette, IN 47907; dcanales@purdue.edu

†Ph.D. Student, School of Aeronautics and Astronautics, Purdue University, West Lafayette, IN 47907; gupta208@purdue.edu

‡MSc. Student, School of Aeronautics and Astronautics, Purdue University, West Lafayette, IN 47907; park1103@purdue.edu

§Hsu Lo Distinguished Professor of Aeronautics and Astronautics, School of Aeronautics and Astronautics, Purdue University, West Lafayette, IN 47907; howell@purdue.edu

to return to Earth.[9] Likewise, some low-thrust analysis has also been introduced for the exploration of both moons.[10] Another commonly proposed approach is a three-staged Mars orbit insertion towards an orbit similar to that of Deimos or Phobos, with Mars at its focus.[11,12] Additionally, Phobos/Deimos resonant gravity assists have also been exploited to explore both moons.[13]

Capture options in the vicinity of Phobos and Deimos are potentially accomplished by leveraging multi-body dynamics techniques to understand the motion in the vicinity of the moons. Since Phobos is frequently the primary target for a number of the previous missions, the motion in its vicinity is explored by various authors. Prior research results are available that explore potential science orbits under the gravitational influence of both Mars and Phobos. In particular, retrograde orbits around Phobos that exist in the Mars-Phobos circular restricted three body problem (CR3BP) are computed and assessed for their stability by Canalias et al.,[14] Chen et al.,[15] as well as Wallace et al.[16] Periodic orbits are also computed within the context of the Mars-Phobos elliptic restricted three body problem (ER3BP), incorporating the irregular gravitational field of Phobos, by Zamaro et al.,[17] and Wang et al.[18] These previous works demonstrate that the inclusion of both the Mars and Phobos gravity fields is a key component in the computation of Phobos science orbits that could potentially be transitioned into a higher-fidelity model for an actual mission scenario.

The complex construction of transfers between moons in a multi-body environment is the focus of numerous previous investigations. It is demonstrated by various authors that low-energy transfers between two distinct moons orbiting a common planet can be successfully achieved using invariant manifolds.[19–21] While most of these studies assume that the moons are in co-planar orbits, strategies to produce transfers between spatial periodic orbits corresponding to two different moons located in their true orbital planes are also available.[21] Such schemes are most often demonstrated in multi-moon systems where the masses of the moons and their relative distances enable these transfers, e.g., the Jupiter or Uranus systems. However, due to the small masses of Phobos and Deimos, the invariant manifold trajectories emanating from orbits near these moons do not intersect in configuration space. Thus, it is difficult to plan potential exploration missions targeting both moons using libration point orbits; typical transfers from one moon to the other are generally expensive in terms of propellant. Furthermore, the gravitational influence of the moons on the s/c is so small that capture scenarios that rely solely on resonant gravity assists via Tisserand graphs[22,23] present significant challenges without extra maneuvers ($\Delta V$s).

The current investigation proposes an alternative mission scenario that includes Mars-Deimos resonant orbits (ROs) for exploring both moons with some reduced propellant costs. The exploration via Mars-Deimos resonant orbits is twofold: (i) repeated Deimos flybys, and (ii) relatively low cost access to Phobos science orbits. The resonant orbits that fulfill these requirements are, thus, introduced. Resonant orbits computed in the Mars-Deimos CR3BP offer periodic Deimos flybys.[24] For this analysis, Phobos science orbits are assumed to be periodic libration point orbits within the context of the Mars-Phobos CR3BP. Mars-Deimos resonant orbits that allow for an intersection with the invariant manifolds arriving into the Phobos science orbits are presented as candidates given their low $\Delta V$s. Both moons are modeled in their true orbital planes at a given epoch. While prior work relevant to this investigation focuses on the s/c arriving at an orbit with the same properties as the orbit of the target moon, in this current work, the Phobos science orbit is assumed to be a Lyapunov orbit. Thus, this investigation is focused on selecting candidate resonant orbits in the Mars-Deimos CR3BP that offer repeated Deimos flybys, and assessing the costs for transfers into the Phobos science orbit.

The dynamical models to fulfill the objectives of this investigation are first introduced, followed

by the assumptions for arrival to the Martian system. Then, a background on resonant orbits computed in the Mars-Deimos CR3BP is presented. The methodology employed for the selection of candidate resonant orbits that provide access to Phobos and Deimos is introduced, and an impulsive as well as a low-thrust analysis of the transfers is completed. The transfers involving resonant orbits that offer repeated Deimos flybys and offer access to Phobos are then analyzed in a higher-fidelity ephemeris model. Finally, some concluding remarks are offered.

## DYNAMICAL MODELS

The Martian system is a multi-body environment with two moons. Despite the fact that the masses of Phobos and Deimos are small, a s/c traversing the system is still subject to the gravitational accelerations due to several bodies simultaneously. For the purposes of this investigation, the CR3BP is leveraged for computing resonant orbits in the Mars-Deimos system, and for computing periodic orbits in the vicinity of $L_2$ in the Mars-Phobos system. Additionally, two variants of the CR3BP are introduced: a patched 2BP-CR3BP model to locate transfers between resonant orbits and the vicinity of Phobos, and a CR3BP with a low-thrust model (CR3BP-LT) for further analysis. Transfers leveraging these models are then validated in a higher-fidelity ephemeris model, accommodating both impulsive and low-thrust propulsion.

### Circular Restricted Three-Body Problem

The CR3BP builds upon insights from the two-body model, while also incorporating some of the complexities of the $\mathcal{N}$-body model. For the purposes of this investigation, the three bodies that comprise the model includes Mars, either one of its moons, and the s/c. The s/c is assumed to possess infinitesimal mass relative to Mars and its moons. Additionally, it is assumed that Mars and Phobos/Deimos move in circular orbits relative to their mutual barycenter. Considering the eccentricities of the orbits of Phobos and Deimos around Mars, equal to $0.0151$ and $0.0002$, respectively, this assumption for circular moon orbits allows the CR3BP to serve as a reasonable approximation of the true dynamics governed by Mars and either of the moons. The orbital planes of the moons are defined by the appropriate epoch in the Mars-centered Ecliptic J2000 frame, but the moons move in their respective circular orbits in their recognized orbital planes. The specifics of the CR3BP are formulated within the context of the Mars-Phobos or Mars-Deimos systems. Note that the moon refers to either Phobos or Deimos.

A rotating frame, represented as $\hat{x}$-$\hat{y}$-$\hat{z}$, is defined such that it rotates with the motion of Mars and its moon; the origin of this frame is located at the Mars-moon system barycenter. It is convenient to nondimensionalize the equations of motion for the s/c in the CR3BP, resulting in an autonomous system that provides greater insight into a range of design problems. The following quantities are defined: the characteristic length, defined as the distance between Mars and the moon, and the characteristic time, determined such that the nondimensional mean motion of the two bodies is equal to one. Additionally, the nondimensional mass ratio is defined as $\mu = m_{P_2}/(m_{P_1} + m_{P_2})$, where $m_{P_1}$ and $m_{P_2}$ denote the masses of Mars and its moon, respectively. Note that the mass ratios of the Mars-Phobos and Mars-Deimos CR3BP systems are $\mu_{MP} = 1.6548 \times 10^{-8}$ and $\mu_{MD} = 0.2245 \times 10^{-8}$, respectively. The nondimensional position vector locating the s/c relative to the system barycenter is defined as $\bar{r}_{s/c} = x\hat{x} + y\hat{y} + z\hat{z}$, where the overbars indicate vector quantities. The nondimensional equations of motion for the s/c then, expressed in terms of the

rotating frame, take the form,

$$\ddot{x} - 2\dot{y} = \frac{\partial U^*}{\partial x}, \quad \ddot{y} + 2\dot{x} = \frac{\partial U^*}{\partial y}, \quad \ddot{z} = \frac{\partial U^*}{\partial z} \tag{1}$$

where the dots indicate the derivative with respect to nondimensional time. Here, the pseudo-potential function is computed as $U^* = \frac{1-\mu}{d} + \frac{\mu}{s} + \frac{(x^2+y^2)}{2}$, where the distance between Mars and the s/c is $d = \sqrt{(x+\mu)^2 + y^2 + z^2}$, and the distance between the moon and the s/c is evaluated as $s = \sqrt{(x-1+\mu)^2 + y^2 + z^2}$. There exists a constant of the motion, i.e., an energy-like quantity formulated in the rotating frame, denoted the Jacobi constant, computed as $JC = 2U^* - (\dot{x}^2 + \dot{y}^2 + \dot{z}^2)$. Additionally, five equilibrium solutions exist in the CR3BP, also termed the libration points. Three of the libration points, namely $L_1$, $L_2$, $L_3$, are collinear and lie along the rotating $\hat{x}$-axis. The remaining two points, $L_4$ and $L_5$, form equilateral triangles with Mars and the moon, in the primary plane of motion as viewed in the rotating frame. Knowledge of the locations of the libration points allows insight into the system dynamics relative to these solutions. In the vicinity of the libration points, periodic solutions exist, such as the planar Lyapunov and the spatial halo orbits. The computation of one periodic solution in the CR3BP guarantees the existence of a family of periodic solutions. The process of natural parameter continuation is employed to generate families of such solutions that possess similar characteristics. Relevant to this investigation, the $L_2$ Lyapunov and $L_2$ halo orbit families in the Mars-Phobos system are computed and further explored to offer access to Phobos. Given periodic orbits in the CR3BP, the knowledge of the flow structures associated with such solutions is leveraged for trajectory design. In particular, stable and unstable manifolds associated with periodic orbits are computed and exploited in the search for connections between different periodic solutions.

*Patched 2BP-CR3BP Model* The spatial patched 2BP-CR3BP model[21] approximates trajectories modeled in either the CR3BP or the 2BP depending on the location of the s/c in the system. Within a certain threshold distance from the moon, the trajectory is modeled with the CR3BP. At such a distance, a sphere of influence (SoI) is defined as a sphere surrounding the moon where the gravitational influence of the moon is considerably high. In this investigation, this distance, or the radius of the SoI, is computed at the location along the $\hat{x}$ axis where the ratio of the gravitational accelerations due to the two primaries is equal to $10^{-5}$, or $x_{SoI} = \ddot{r}_{moon}/\ddot{r}_{Mars} = 5 \cdot 10^{-5}$. $x_{SoI}$, denotes the ratio of acceleration, where $\ddot{r}_{moon}$ and $\ddot{r}_{Mars}$ correspond to the gravitational accelerations due to the moon and Mars, respectively. When the trajectories pass beyond the SoI, the motion is approximated as Keplerian with a focus at the larger primary and uniquely determined by the osculating orbital elements: semi-major axis ($a$) , eccentricity ($e$), right ascension of the ascending node ($\Omega$), inclination ($i$), argument of periapsis ($\omega$) and true anomaly ($\theta$). For example, assume a trajectory is desired that arrives into the vicinity of Phobos. From an orbit in the Mars-Phobos system, the state is propagated backwards in time in the CR3BP towards the Phobos SoI, where the state is instantaneously defined as a back-propagated Keplerian orbit in the inertial frame, with Mars at its focus (see Figure 1 for a schematic). Simultaneously, there exists a Keplerian orbit approaching from Deimos. An analytical exploration of the potential intersection of the two conics is possible since trajectories departing Deimos and arriving at Phobos are blended into the Ecliptic J2000 Mars-centered inertial frame. A strategy based in the spatial patched 2BP-CR3BP algorithm then blends the arcs into an end-to-end transfer as detailed by Canales et al.,[21] incorporating maneuvers as necessary. Given the relatively small masses of both Deimos and Phobos, results are readily transitioned to the higher-fidelity ephemeris model as well.

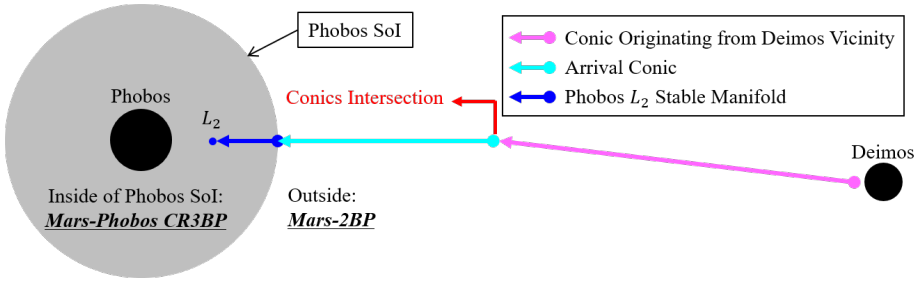


**Figure 1. Scheme representing the blending of two different systems in the Ecliptic J2000 planet-centered inertial frame according to the patched 2BP-CR3BP model.**

*CR3BP-LT Model* For the analysis of the low-thrust engine model within the context of the CR3BP, an additional acceleration term is added to the right side of Eq. (1). This term is $\bar{T}/m$, where $\bar{T}$ is the low-thrust force and $m$ is the mass of the s/c. Since $m$ also depends on time, it is incorporated into Eq. (1) as follows,

$$\ddot{x} - 2\dot{y} = +\frac{\partial U^*}{\partial x} + \frac{T_x}{m}, \quad \ddot{y} + \dot{x} = +\frac{\partial U^*}{\partial y} + \frac{T_y}{m}, \quad \ddot{z} = \frac{\partial U^*}{\partial z} + \frac{T_z}{m}, \quad \dot{m} = -\frac{T}{g_0 I_{sp}} \tag{2}$$

where the low-thrust force components acting along the $\hat{x}, \hat{y}, \hat{z}$ directions are $T_x, T_y, T_z$, respectively. The magnitude of the thrust vector, $\bar{T} = T$, is between 0 and $T_{max}$. The value of the specific impulse, $I_{sp}$, is assumed to be constant and, together with the standard gravity acceleration $g_0 = 9.80665 m/s^2$, these parameters determine the mass flow rate $\dot{m}$.

### Higher-Fidelity Ephemeris Model

The higher-fidelity ephemeris model represents the motion of a s/c subject to multiple gravitational accelerations. The motion of a s/c of mass $m_i$ is modeled relative to a central body of mass $m_q$. Located relative to the central body, $N$ perturbing bodies of mass $m_j$ for $j = 1, \ldots, N$, are also incorporated in the model. In this model, all the bodies are assumed to be centrobaric point masses. This implementation relies on the SPICE libraries[25] supplied by the Ancillary Data Services of NASA's Navigation and Ancillary Information Facility (NAIF), through which precise positions and velocities are retrieved. The dimensional acceleration acting on the s/c in a model with $N$ perturbing bodies is then expressed as,

$$\ddot{\bar{r}}_{q-i} = \frac{-G(m_i + m_q)}{r_{q-i}^3}\bar{r}_{q-i} + G\sum_{j=1}^{N} m_j \left( \frac{\bar{r}_{i-j}}{r_{i-j}^3} - \frac{\bar{r}_{q-j}}{r_{q-j}^3} \right) + \frac{\bar{T}}{m}, \tag{3}$$

where $i$ denotes the s/c, $q$ denotes the central body, and $j$ corresponds to the perturbing bodies. The gravitational constant is denoted by $G$, and the dots in the equation represent derivatives with respect to dimensional time. Note that $\bar{r}_{o-f}$ represents the position vector of body '$f$' relative to body '$o$', where the subscripts $o$ and $f$ are $i$, $q$ or $j$, as apparent in Eq. (3). In this investigation, the transfers obtained using the CR3BP models are validated in a higher-fidelity ephemeris model that includes the s/c, Mars, Sun, Phobos, Deimos and Jupiter. For the low-thrust engine model, the acceleration from the low-thrust force, $\bar{T}/m$, is incorporated as well.

## ARRIVAL INTO THE MARTIAN SYSTEM

The main goal of this investigation is an approach that yields access to Deimos and Phobos given their orbits as represented in Table 1. Of course, any trajectory to Mars is constrained by the

departure state from the Earth vicinity and an optimal arrival to the Mars or the moon science orbit cannot be separated from the Earth departure. Thus, given the extensive prior analysis of the Earth-to-Mars transfer problem, impulsive transfers to the Martian system are beyond the scope of this investigation, although it is noted that a three-stage Mars orbit insertion strategy is a typical arrival approach.[11,12] However, some assumptions regarding low-thrust propulsion can be leveraged to simplify the arrival state into the Martian system.

**Table 1. Orbital data of Phobos and Deimos obtained from the SPICE database[25] in the Ecliptic J2000 reference frame. Last accessed 08/05/2020. $a$ is semi-major axis, $P$ is the orbital period, $e$ is the eccentricity, $i$ is the inclination, and $\Omega$ is the right ascension of the ascending node (RAAN). $i$ and $\Omega$ are computed with respect to the Mars J2000 equatorial plane.**

| | $a$ [km] | $P$ [hour] | $e$ [nd] | $i$ [°] | $\Omega$ [°] |
|---|---|---|---|---|---|
| Phobos | $9,377.82$ | 7.65 | 0.01482 | 1.05 | 131.71 |
| Deimos | $23,459.61$ | 30.29 | 0.00019 | 2.44 | 260.12 |

Interplanetary low-thrust trajectories are a function of interdependent parameters associated with the mission architecture, engine specifications and time of flight. The arrival state of the s/c to the Martian system is also dependent on these parameters. The Earth departure options include a dedicated launcher with a considerable characteristic energy ($C_3$) with respect to the Earth, and a launch as a secondary payload on other interplanetary/geocentric missions; these various options govern the initial state of the s/c and, thus, render a broad range for the optimal state for arrival to the Martian system. For this investigation, the arrival state is conveniently defined by utilizing the history of the energy-like Jacobi constant in the Sun-Mars system, $JC_{SM}$, of the low-thrust Earth-to-Mars trajectories. A sample scenario is selected and the resulting trajectory is generated using the higher-fidelity ephemeris model, as shown in Figure 2(a). The trajectory departs from the vicinity of the Earth at a location $4 \times 10^5$ km away from the Earth and arrives at a Mars-centered circular orbit in the Sun-Mars J2000 ecliptic plane with an orbital radius equal to that of Deimos. Figure 2(b) illustrates the history of the Jacobi constant in the Sun-Mars CR3BP system, $JC_{SM}$, corresponding to the transfer trajectory. Although this trajectory illustrates one specific scenario, the time history for $JC_{SM}$ in the low-thrust Earth-to-Mars transfer trajectories must generally exhibit the characteristics in Figure 2(b). First, the $JC_{SM}$ along the Earth-to-Mars transfer arc must be lower than that of the Sun-Mars $L_1$ libration point to enable the s/c to enter the Martian system. Additionally, the $JC_{SM}$ for a destination orbit near Mars in the Sun-Mars system must be higher than that of the Sun-Mars $L_1$, $JC_{SM,L_1}$, to ensure capture by the second primary. Therefore, all candidate orbits possess a $JC_{SM}$ value greater than $JC_{SM,L_1}$. Contrary to impulsive engines, low-thrust engines change the velocity and energy of the s/c continuously. Thus, the $JC_{SM}$ of the states of the s/c along the transfer trajectory must be lower than $JC_{SM,L_1}$ while approaching the Martian system, and it must be continuously raised to the final $JC_{SM}$ of the destination orbit. Without any loss of generality, it is assumed that the tentative arrival state in the Martian system is associated with a $JC_{SM}$ smaller than $JC_{SM,L_1}$. In this investigation, the $JC_{SM}$ at the tentative arrival state is assumed to be 3.00018, a value that is slightly lower than $JC_{SM,L_1} = 3.00020$ to ensure that the trajectory passes through the $L_1$ libration point gateway. The energy difference between this value and the $JC_{SM}$ of the various candidate science orbits is a useful indicator of the associated propellant costs, as the Sun and Mars are the dominant gravitational bodies upon arrival, and the Jacobi constant is adjusted only by the low-thrust maneuvers. This assumption is analogous to fixing the arrival state such that $v_\infty = 0$, consistent with the Mars two-body model, which is a common practice when generating preliminary trajectories.[26]

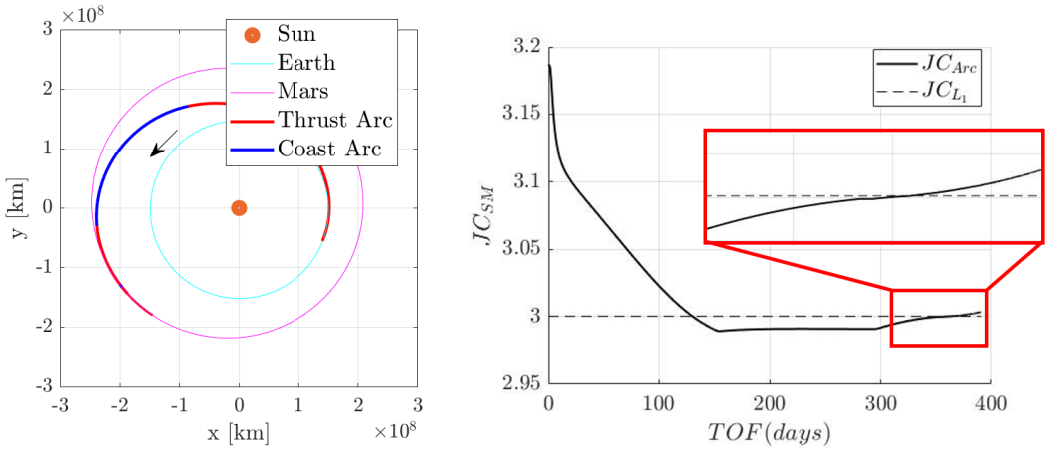


(a) Sun-centered inertial frame view

(b) $JC_{SM}$ history

**Figure 2. A sample low-thrust Earth-to-Mars transfer trajectory and energy ($JC_{SM}$) history. Departure on 08/31/24, arrival on 09/27/25.**

The specifications of the s/c are selected to be consistent with the values that appear in previous investigations. Upon the arrival across all resonant orbits, the mass of the s/c is assumed to be $m_0 = 180\ kg$, a realistic value when the s/c departs from an Earth geostationary transfer orbit as a secondary payload on the EELV Secondary Payload Adapter (ESPA) ring[27] with a low-thrust engine. Then, the propellant costs between the different resonant orbits and the Phobos science orbit are measured as the consumed mass from this consistent value. The model for the low-thrust engine assumes a maximum thrust level of $T_{max} = 60\ mN$, and a specific impulse such that $I_{sp} = 3000\ s$. These values are comparable to those in prior investigations for Earth-Mars transfers with ballistic escape and low-thrust capture.[28] Both sets of parameters produce similar levels of maximum acceleration ($3.3 \times 10^{-4}\ m/s^2$ vs. $2.5 \times 10^{-4}\ m/s^2$) with the same specific impulse value. Despite the assumptions regarding the arrival state and the s/c specifications, the results from this investigation are extendable.

## RESONANT ORBITS BACKGROUND

The proposed mission scenario entails that the s/c completes repeated Deimos flybys, while also providing access to Phobos. To that end, resonant orbits are computed and assessed for their applicability to this investigation. Resonant orbits have an extensive history for planetary flybys, and the invariant manifolds of unstable resonant orbits are applied frequently towards transfer trajectory design. Additionally, mission designs leveraging the inherent stability of some resonant orbits are conceptualized and successfully applied to long-term mission scenarios. For example, the Interstellar Boundary Explorer (IBEX), originally launched in 2008 into a highly elliptical orbit around the Earth, was later transferred into a spatial $3:1$ resonant orbit, thereby guaranteeing long-term stability.[29] Following, in 2018, the Transiting Exoplanet Survey Satellite (TESS) was launched directly into an operationally stable spatial $2:1$ resonant orbit.[30] This investigation exploits the stability of resonant orbits, coupled with their distinctive repeating geometry, as visualized in a rotating frame.

Prior to computing resonant orbits in the Mars-Deimos CR3BP system, resonant orbits are computed in the two-body model such that the s/c orbiting Mars is in resonance with Deimos. In the two-body model, the relationship between the orbital periods of the s/c and Deimos, which are denoted as $T_{s/c}$ and $T_D$ respectively, is expressed as $p/q = T_D/T_{s/c}$. The integer $p$ represents the

number of revolutions completed by the s/c around Mars, and $q$ represents the number of revolutions completed by Deimos in the same time interval. The s/c is then in $p:q$ resonance with Deimos. For instance, a s/c in $3:4$ resonance with Deimos around Mars completes three revolutions in the time that Deimos requires to orbit Mars four times. Visualizing this orbit in the Mars-Deimos rotating frame reveals the characteristic loops associated with resonant orbits. The number of loops that appear in this frame corresponds to the value of $p$ in the associated $p:q$ resonance ratio.

The two-body resonant orbits are then transitioned to the Mars-Deimos CR3BP model, noting the following distinction: due to the additional gravitational forces in this model, the resulting resonant orbit no longer possesses a perfect integer resonance ratio with Deimos. Therefore, in the Mars-Deimos CR3BP system, the $p:q$ resonance ratio implies that the s/c completes $p$ revolutions in *approximately* the time that Deimos completes $q$ revolutions around Mars. Additionally, the transitioned orbit is no longer precisely periodic and thus, differential corrections techniques are employed to produce the analogous periodic resonant orbit in the CR3BP. Utilizing the initial conditions corresponding to the two-body resonant orbit, a single-shooting targeting scheme is applied to converge an equivalent resonance in the CR3BP.[31]

For this investigation, a variety of resonant orbits in the Mars-Deimos system are examined, including the planar $2:1$, $2:3$, $3:2$, $3:4$, $3:5$, $4:3$, $5:3$, and $5:4$ orbit families. Spatial resonances belonging to the $2:3$, $3:2$, $3:4$, $4:1$, and $4:3$ resonant orbit families are evaluated as well. Figures 3 and 4 highlight the distinctive geometries possessed by various planar and spatial orbits corresponding to different resonance ratios in the Mars-Deimos system. For clarity concerning the robustness of the expected geometries for these resonant orbits, individual orbits are also propagated in the higher-fidelity ephemeris model. Specifically, the orbits are transitioned from the Mars-Deimos CR3BP model to the Mars-Deimos-Phobos-Sun-Jupiter ephemeris model. With the epoch as 11/22/2020 22:00:00, the initial states corresponding to various resonances are propagated for approximately 30 days. As a demonstrative example, the results from propagating a $2:1$ and a $3:2$ resonant orbit are illustrated in Figure 5. As is apparent, the orbits maintain their geometry without any significant deviations, and remain bounded to the base-orbit computed in the CR3BP. Thus, these stable orbits are considered as Deimos science orbit candidates.

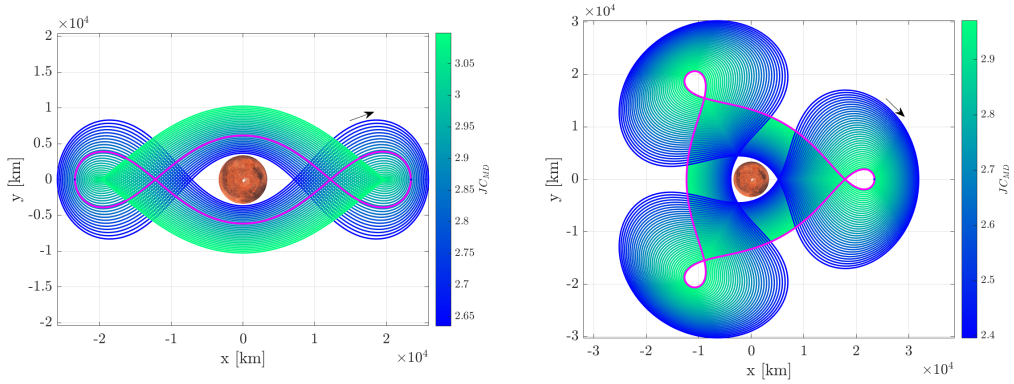


(a) $2:1$ resonant orbits.

(b) $3:2$ resonant orbits.

**Figure 3. Representative members from the planar $2:1$ and $3:2$ resonant orbit families in the Mars-Deimos CR3BP system. The magenta arcs are the candidates $2:1$A and $3:2$B that are further investigated.**

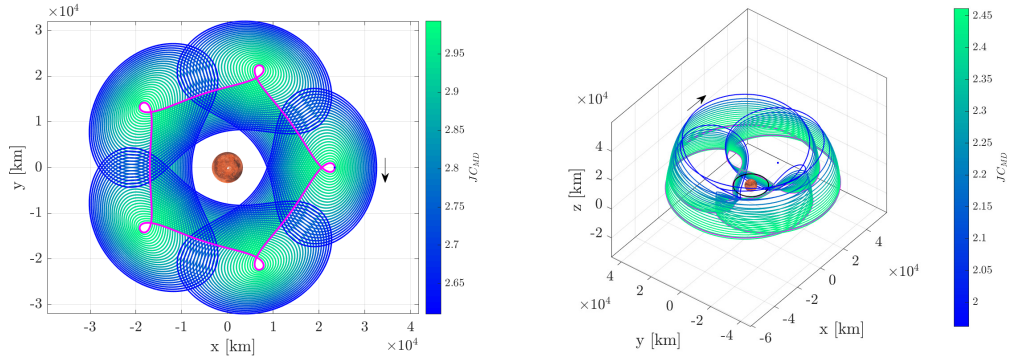


(a) $5:4$ resonant orbits. (b) $3:4$ resonant orbits.

**Figure 4. Representative members from the planar $5:4$ and spatial $3:4$ resonant orbit families in the Mars-Deimos CR3BP system. The magenta arc is the candidate $5:4$B orbit that is further analyzed in Figure 14.**

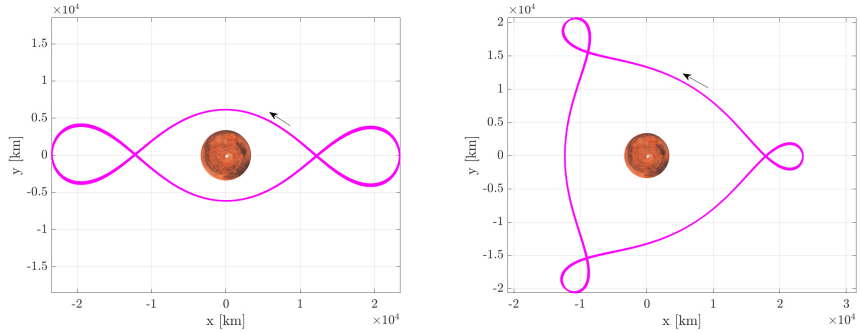


(a) $2:1$ resonant orbit. (b) $3:2$ resonant orbit.

**Figure 5. Propagation of a $2:1$ and a $3:2$ resonant orbit for 30 days. Model: higher-fidelity ephemeris model. Epoch: 11/12/2020 22:00:00.**

## RESONANT ORBITS WITH ACCESS TO PHOBOS AND DEIMOS

Given the cost and challenges of sending a s/c from Earth to the moons of Mars, it is convenient to find orbits in the Martian system that aid with the exploration of both Phobos and Deimos. Given the advantages that resonant orbits offer in the Mars-Deimos system, these orbits are considered to link arrival states into the Martian system to the desired science orbits in the Phobos vicinity. With this objective in mind, the most important requirement for the selection of the desirable resonant orbits is identifying orbits that permit access to Phobos and, in particular, the Phobos science orbits. Thus, the target Phobos science orbits are initially defined. Given the small variation in the Mars-Phobos Jacobi constant ($JC_{MP}$) along the $L_2$ families for both the Lyapunov and halo periodic orbits in the Mars-Phobos CR3BP system, the arrival $\Delta V$ at any orbit along either family is similar, since $JC_{MP}$ indicates the energy level of the science orbits. For example, representative members from the family of the $L_2$ Lyapunov and halo orbits in the Mars-Phobos rotating frame are plotted in Figure 6, where each orbit is colored according to the nondimensional value of its $JC_{MP}$. An $L_2$ Lyapunov orbit possessing a Jacobi constant value equal to 3.000023 is selected as the Phobos science orbit, as highlighted in Figure 6(a). From this Lyapunov orbit, a stable manifold trajectory

is propagated in reverse time towards the Phobos SoI, where it becomes a back-propagated arrival conic. Then, given that the resonant orbit and the arrival conic are not in the same plane, the patched 2BP-CR3BP model is used to construct spatial intersections with the resonant orbit.[21] Although the selected Lyapunov orbit is planar, the associated costs are extendable to a spatial halo orbit given the small variations in $JC_{MP}$.

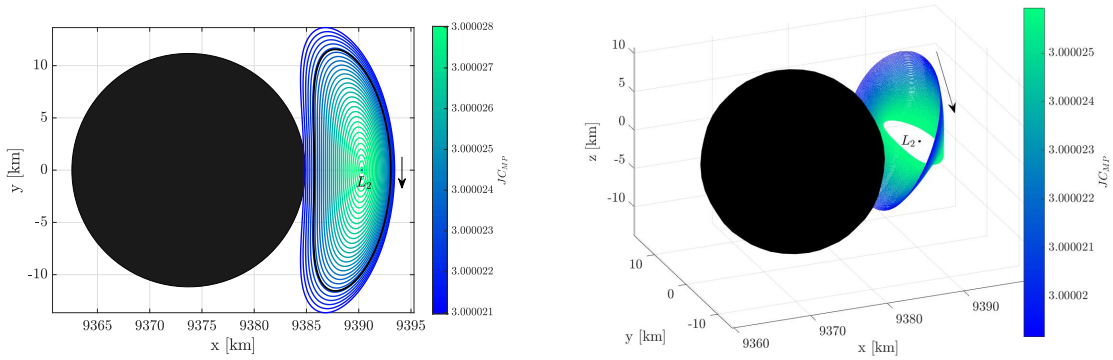


(a) Mars-Phobos $L_2$ Lyapunov family.

(b) Mars-Phobos $L_2$ Halo family.

**Figure 6. $L_2$ Lyapunov and halo orbits families in Mars-Phobos CR3BP system. In black, the arrival $L_2$ Lyapunov periodic orbit with $JC_{MP} = 3.000023$ is highlighted. Phobos is assumed to be perfectly spherical in this investigation and appears in black.**

To compute impulsive transfers from any resonant orbits to the arrival moon vicinity, the Moon-to-Moon Analytical Transfer method (MMAT)[21] is leveraged. One of the main challenges in constructing transfers between two moons is determining the conditions such that they can occur and the relative phase between moons in their respective planes is one of the key elements. Employing the MMAT approach, an intersection in configuration space between the given resonant orbit and the arrival conic is determined if available. As a result, for a given departure angle relative to Deimos, the location of Phobos at arrival is delivered such that the intersection between the resonant orbit and arrival conic is guaranteed. At the initial time of the transfer, the s/c is assumed to be located at a desired point along the Mars-Deimos resonant orbit. Given that the resonant orbit is computed for the Mars-Deimos CR3BP, its argument of periapsis is selected such that the apoapsis of the resonant orbit is directed towards Deimos at instant 1. Thus, the argument of periapsis of the resonant orbit is related to the true anomaly of Deimos in its orbit at the origin of the transfer to Phobos, $\theta_{0_{Dei}}$, which is measured from the Deimos orbit's right ascension of the ascending node (RAAN). Recall that the orbit of Deimos is approximated as circular. Note that instant 1 refers to the moment that the transfer from the resonant orbit towards the vicinity of Phobos originates. Figure 7 illustrates the orientation of the resonant orbit with respect to the orbital plane of Deimos for different $\theta_{0_{Dei}}$. Two different examples are illustrated with the two angles $\theta_{0_{Dei,1}}$ and $\theta_{0_{Dei,2}}$ in Figure 7. Note that, in the schematic, the s/c is assumed to depart towards Phobos at the apoapsis of the resonant orbit.

The objective is to determine whether a transfer between the resonant orbit and the Phobos vicinity is available. The true anomaly of Deimos in its orbit at instant 1, $\theta_{0_{Dei}}$, is considered fixed. Note that the departure conic can be defined as either the same resonant orbit approximated in the Mars-2BP or an intermediate conic that joins the resonant orbit with the arrival conic. Both options are extensively explained below. Spatial intersections between the departure and arrival conics occur

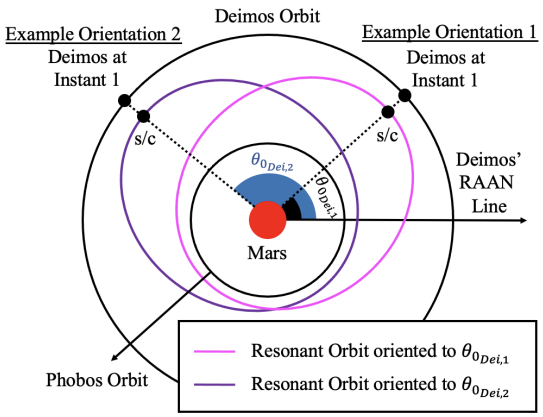


**Figure 7. Scheme that represents the location of the s/c and the resonant orbit with respect to Deimos depending on $\theta_{0_{Dei}}$. Then, $\theta_{0_{Dei},1}$ and $\theta_{0_{Dei},2}$ represent two different sample epochs at instant 1 assuming that the s/c departs towards Phobos at the apoapsis of the resonant orbit.**

if and only if the following analytical condition is satisfied. The condition must be fulfilled such that the arrival conic is re-phased, or re-oriented, to deliver a spatial intersection between the arrival conic and the departure conic:[21]

$$a_a(1-e_a) \leq \frac{a_d(1-e_d^2)}{1+e_d\cos(\theta_{d_{Int}}+n\pi)} \leq a_a(1+e_a), \text{ being } n=0,\ 1, \tag{4}$$

where $a_a$ and $a_d$ are the semi-major axes of the arrival conic and the resonant orbit, respectively; $e_a$ and $e_d$ are the eccentricities of the arrival conic and the resonant orbit, respectively; and the angle $\theta_{d_{Int}}$ or $\theta_{d_{Int}}+\pi$ correspond to the true anomaly of the departure conic when it intersects with the arrival plane, measured from the argument of periapsis, $\omega_d$. Recall that the angle $\theta_{d_{Int}}$ is generally defined by the values of the inclination, $i$, and the right ascension of the ascending node angle, $\Omega$, for the departure and arrival planes, as well as the argument of periapsis for the resonant orbit, $\omega_d$. Note that $\omega_d$ depends upon the initial epoch at the origination of the transfer with respect to Deimos, $\theta_{0_{Dei}}$. If the inequality constraint in Eq. (4) is satisfied, the unique phase for Phobos that yields such a configuration is produced. Then, the process is repeated for every value of $\theta_{0_{Dei}}$ over an entire period of Deimos in its orbit, i.e., all available phases for Deimos in its orbit measured from $\Omega$ over an entire period. The configuration of the two moons, or the relative orientation between Phobos and Deimos, that provides the minimum analytical $\Delta V$ is determined. The total time of flight, $t_{TOF}$, is also evaluated. Given that the MMAT method is applied to generate transfers between resonant orbits and the vicinity of Phobos, the transfers are divided into two different types depending on the conic arc used to assess Eq. (4): (1) direct transfers from the resonant orbit to the arrival conic, and (2) two-burn transfers, that incorporate an intermediate arc to link the resonant orbit with the arrival conic, as represented in Figure 8.

### Case 1: Direct Transfers

As is evident in Figure 9, the higher the value of the Mars-Deimos Jacobi constant, $JC_{MD}$, corresponding to the resonant orbit in its associated orbit family, the lower the minimum $\Delta V$ obtained in the feasibility analysis for a direct transfer to Phobos. As an example, Figure 9 illustrates the evolution of the $\Delta V$ for a direct transfer to Phobos for the $3:2$ and the $5:4$ planar families as a function of the $JC_{MD}$ of the resonant orbit. Therefore, Eq. (4) is evaluated across the resonant

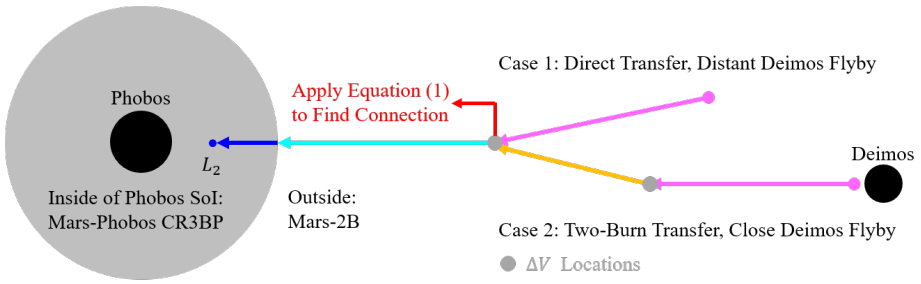


**Figure 8. Two types of scenarios for the construction of transfers between resonant orbits and a periodic orbit in the vicinity of $L_2$ in the Mars-Phobos system.**

orbit family for every $\theta_{0_{Dei}}$ of Deimos in its orbit. If Eq. (4) is satisfied, then the minimum $\Delta V$ configuration between Phobos and Deimos is produced. Then, the orbit with the maximum $JC_{MD}$ value that supplies access to Phobos is selected. As a result, the candidates for resonant orbits in the Mars-Deimos system are reduced to members from the planar $3:2$, $3:4$, and the $5:4$ families, and orbits from the spatial $3:4$ resonant orbits. Figure 10(a) illustrates an example of a direct transfer from the spatial $3:4$B resonant orbit. These results are summarized in the first four rows of Table 2 under Case 1. A s/c in these resonant orbits can access Phobos with only one maneuver, hence the arc is denoted as a direct transfer. Additionally, the orbits provide the opportunity to conduct flybys of Phobos, given their proximity to its orbit. Recall that the numbers 1-4, which denote the locations of the two moons at instants along the transfer as represented in Figure 10(a), are defined in Figure 8. Also, for reference, these instants are defined in the same way as Canales et al.[21]

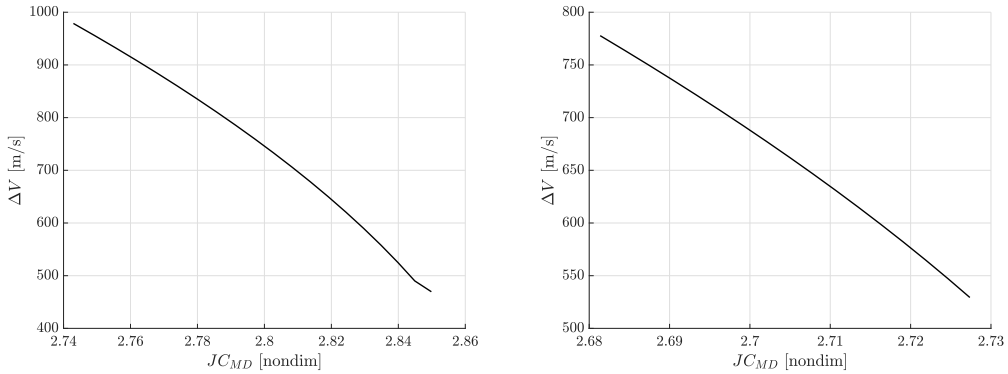


(a) Evolution in the 3:2 resonant orbit family.

(b) Evolution in the 5:4 resonant orbit family.

**Figure 9. Evolution of the $\Delta V$ magnitude with respect to $JC_{MD}$ for a direct transfer to Phobos for the $3:2$ and the $5:4$ planar families.**

### Case 2: Two-Burn Transfers

The selected resonant orbits for Case 1 do not offer close Deimos flybys. To reach Deimos, an intermediate conic arc is incorporated, as represented by the orange arc in Figure 8, to bridge the gap from the resonant orbits to Phobos while guaranteeing that close Deimos flybys are available. Thus, the semi-major axis of the resonant orbit, $a_d$, is adjusted such that the flybys with Deimos occur at relatively closer distances. Then, to decrease the $\Delta V$ for the extra maneuver, this intermediate conic arc departs from the apoapsis of the resonant orbit and targets a periapsis that equates to that of the arrival conic. Note that this strategy does not correspond to a Hohmann transfer since the

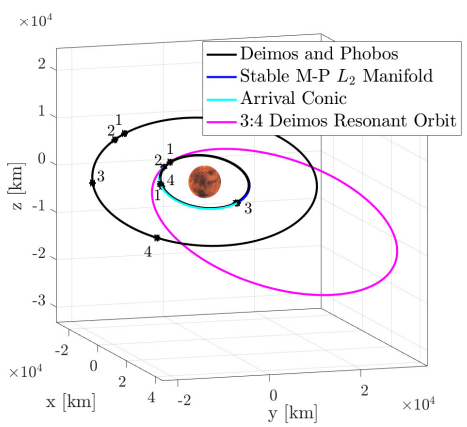


(a) Case 1: Transfer from $3:4$B resonant spatial orbit. $\Delta V_{tot} = 653.4$ m/s, $t_{TOF} = 5.41$ days.

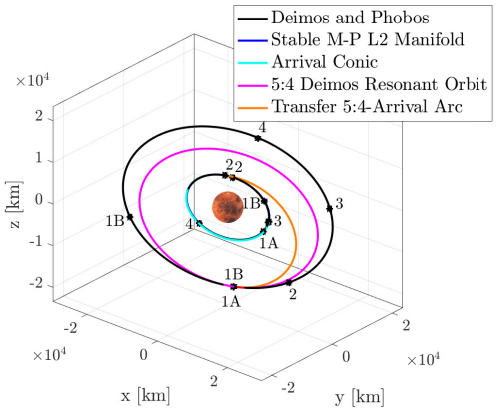


(b) Case 2: Transfer from $5:4$B resonant planar orbit. $\Delta V_{tot} = 643.9$ m/s, $t_{TOF} = 43.74$ hours.

**Figure 10. Sample candidate RO transfers to a Mars-Phobos $L_2$ Lyapunov orbit (Ecliptic J2000 Mars centered inertial frame). Model: 2BP-CR3BP patched model.**

**Table 2. Candidate Resonant Orbits (ROs) belonging to Case 1 (direct transfer, Figure 10(a)), Case 2 (two-burn transfer, Figure 10(b))**

| Candidate ROs | | $x_0$ [nd] | $z_0$ [nd] | $\dot{y}_0$ [nd] | Period [nd] | $\Delta V$ [m/s] | $JC_{MD}$ |
|---|---|---|---|---|---|---|---|
| Case 1 | 3:2A | 1.1200 | N/A | -0.4305 | 12.5664 | 480 | 2.8547 |
| | 3:4A | 0.4005 | N/A | 1.6410 | 25.1327 | 630 | 2.4609 |
| | 3:4B | 0.3991 | 0.0230 | 1.6448 | 25.1327 | 650 | 2.4569 |
| | 5:4A | 1.3199 | N/A | -0.7244 | 25.1327 | 530 | 2.7328 |
| Case 2 | 3:2B | 1.0010 | N/A | -0.1718 | 12.5663 | 528 | 2.9705 |
| | 2:1A | 0.9982 | N/A | -0.3530 | 6.2832 | 580 | 2.8753 |
| | 2:1B | 1.0010 | N/A | -0.3602 | 6.2832 | 582 | 2.8702 |
| | 5:4B | 1.0010 | N/A | -0.0858 | 25.1324 | 643 | 2.9926 |

intermediate and the arrival conics are not contained in the same plane. Yet, given its similarity to a Hohmann transfer, this intermediate arc connecting the resonant orbit and the arrival conic corresponds to a closer minimum $\Delta V$ maneuver for this Case 2. The Keplerian elements of the intermediate arc are now used to evaluate Eq. (4), instead of the resonant orbit orbital elements. This case requires two separate maneuvers, as illustrated by red dots in Figure 8, but the total $\Delta V$ remains comparable to Case 1. Despite the additional $\Delta V$, the new selected resonant orbits possess higher $JC_{MD}$ in their respective families, which results in a lower cost to transfer to Phobos. Along the family of resonant orbits, the orbits that include close Deimos flybys and also satisfy Eq. (4) are added to Table 2 under Case 2. As it was demonstrated in the resonant orbits background section, all the candidate orbits for both cases offer long term stability when transitioned into a higher-fidelity ephemeris model, which is generally desired to meet the scientific requirements. A sample Case 2 transfer from the $5:4$B planar resonant orbit is illustrated in Figure 10(b). Recall that each instant identified in Figure 10(b) is defined in Figure 8.

## LOW-THRUST ANALYSIS OF THE SELECTED RESONANT ORBITS

The costs associated with each candidate resonant orbit, summarized in Table 2, are now transitioned to a low-thrust engine model. Since the thrust level is low, it requires many revolutions around Mars, or a spiral-down arc, to achieve the energy change associated with the transfers. These spiral-down arcs are decomposed into two phases as represented in the schematic in Figure

11: spiral-down (A) and spiral-down (B). The first phase of the arc connects the tentative arrival state, associated with a fixed Sun-Mars Jacobi constant value, $JC_{SM} = 3.00018$, to each resonant orbit. The second phase of arc corresponds to the transfer from each resonant orbit to the sample Phobos science orbit.

### Spiral-Down (A): Anti-Velocity Steering Law

An anti-velocity steering law in Sun-Mars CR3BP is employed to generate spiral-down (A), where the s/c is thrusting with the maximum thrust magnitude in the direction opposite to the rotating velocity. Thus, the low-thrust term in Eq. (2) is evaluated as follows: $\bar{T} = -T_{max}\frac{\bar{v}}{v}$, where $\bar{v}$ denotes the rotating velocity of the s/c. This steering law offers a minimum time of flight for a given difference in $JC$, and is a useful reference value for the cost associated with a specified time of flight and propellant consumption, corresponding to arrival at each resonant orbit. From each resonant orbit, the trajectories are propagated in reverse time with the anti-velocity steering law until the value of the Jacobi constant reaches $JC_{SM} = 3.00018 < JC_{SM,L_1}$, or when the energy is sufficient to open the $L_1$ gateway. Although this strategy offers a limited control over the targeted quantity, it can be coupled with a differential corrections scheme to produce feasible and optimized trajectories from the Earth vicinity to the candidate resonant orbits. Figure 12 illustrates a low-thrust arc connected to a heliocentric leg that enters the Martian system through the Sun-Mars $L_1$ gateway. These orbits serve as an initial guess to generate an end-to-end trajectory, as in Figure 2(a). Thus, the anti-velocity steering law provides useful estimates of the costs associated with arriving at the resonant orbits given the difference in the energy of the s/c along a heliocentric path and the energy of the s/c in the Mars-centered resonant orbits. The corresponding costs for spiral-down (A) are included in Table 3.

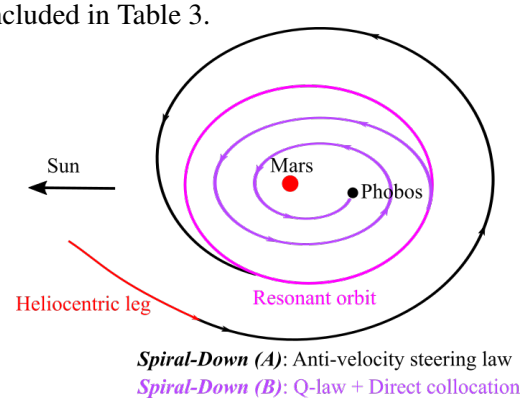


**Figure 11. Two spiral-down strategies schematic**

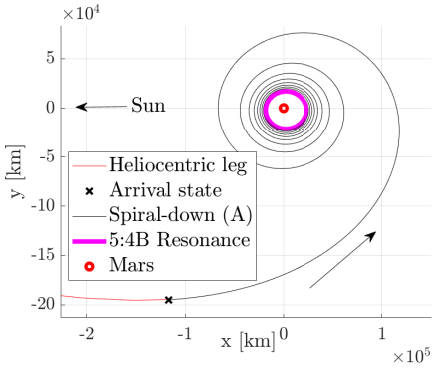


**Figure 12. Spiral-down (A) example**

### Spiral-Down (B): Q-law + Direct Collocation

Other options from each resonant orbit to the Phobos science orbit include an arc with several revolutions, defined as the spiral-down option (B) in Figure 11. Since the resonant orbits are linearly stable as well as periodic, the spiral-down (B) is is solved independently from the spiral-down (A). The main distinction between the (A) and (B) arcs is an additional boundary constraint on the final state along the arc that coincides with the state along the stable manifold of the Phobos science orbit, as represented by the blue line segment in Figure 8. An algorithm capable of incorporating multiple revolutions as well as rendezvous is required, as the state along the manifold changes with the epoch. To that end, a methodology that combines Q-law[32] and direct collocation[33] is developed.

The history of state and control along the spiral-down (B) arc generated by Q-law is introduced as an initial guess for the direct collocation process, by which the rendezvous is achieved and also the trajectory is optimized. Both Q-law and direct collocation are briefly summarized, followed by a step-by-step description of the interface between the algorithms.

*Q-law.* A Q-law control strategy utilizes a candidate Lyapunov function, $Q$, to quantify the distance from the osculating orbital elements to the target orbital elements. The dynamics of the s/c is represented in the Gauss's form of variational equations, by which the time derivatives of the osculating orbital elements are represented as functions of the osculating orbital elements as well as additional forces besides the gravitational force from the central body, Mars in this investigation. While the thrust is assumed to be at the maximum value, the control history of the two thrusting angles is computed at each moment to maximize the decrease of $Q$, which is also labelled the distance quotient. One of the two thrusting angles is measured in the osculating orbital plane with respect to the circumferential direction, assumed to be positive away from the central gravitational body. The other angle is measured from the osculating orbital plane, positive in the direction of the osculating angular momentum. These two angles fully define the three-dimensional thrust vector in the osculating radial, circumferential and angular momentum directions. Although Q-law, in its simplest form, is efficient in generating a possible transfer between two orbits, it fails to target the fast-variable (true anomaly), implying that it cannot pinpoint the exact location along the destination orbit where the s/c arrives at. Moreover, the time of flight along a trajectory generated with Q-law is unknown a priori; thus, the Q-law algorithm by itself cannot handle a rendezvous problem. This poses a problem since in this analysis, for the s/c to arrive at the Phobos science orbit or to encounter Phobos, both the true anomaly of the s/c along the Phobos science orbit at the arrival and the time of flight for the spiral-down arc should be specified. This investigation overcomes this challenge by leveraging direct collocation, and the trajectory generated with Q-law only serves as an initial guess and remains a preliminary transfer solution.

*Direct Collocation.* The direct collocation algorithm used in this investigation is based on the one implemented and extensively explained by Pritchett.[33] A collocation scheme discretizes a continuous trajectory into $s$ segments. While the scheme supports different dynamical models, the higher-fidelity ephemeris model (Equation (3)) is employed and approximated as a polynomial of degree $n$. Formulated with the Legendre-Gauss-Lobatto node placement scheme, the collocation algorithm is equivalent to an implicit Runge-Kutta integration with $(2n-2)^{th}$ order of accuracy.[34] In this investigation, $n = 7$, thus, the dynamics are approximated with $7^{th}$ order polynomials, and are equal to an implicit Runge-Kutta integration of $12^{th}$ order. While classical orbital elements or modified equinoctial elements are potentially available as the state variables, Cartesian position and velocity are employed here. The control variables consist of the magnitude and the direction of the thrust, and are assumed to be constant over a segment. In this investigation, this constant thrust direction is represented in the osculating radial, circumferential and angular momentum directions that are not fixed in the inertial frame. As realistic missions utilize the turn-and-hold strategy for the thrust vector in the inertial directions, it is noted that an extra step may be required to convert the current solutions into a more realistic scenario. The problem formulation also incorporates the following boundary constraints: the s/c originates from a selected resonant orbit at its apoapsis, and the s/c arrives along the stable manifold of the Phobos science orbit at the SoI for Phobos. Then, the feasible state and control history is produced by employing a differential corrections process, and passed to a direct optimization algorithm to solve for mass-optimal trajectories. This approach of pairing collocation and direct optimization is denoted direct collocation.

*Interfacing Q-Law and Direct Collocation.* Recall that the main challenge with a Q-law control approach for the application of the spiral-down (B) scheme is that it fails to target the true anomaly of the s/c upon its arrival at the Phobos science orbit. To address that deficiency, the results from Q-law are now passed to a direct collocation algorithm that not only accommodates the Phobos rendezvous, but also serves as an optimizer. The algorithm that interfaces the Q-law control history and the direct collocation targeting is described with the following steps:

1. The final state, defined as the state along the stable manifold associated with the Phobos science orbit when it crosses the SoI for Phobos, is converted into the osculating orbital elements in the Mars-2BP at an estimated final epoch, $JD_{f,est}$. These elements serve as the target variables for the Q-law guidance process. The position of this final state in a Mars-centered inertial frame is represented as the yellow circle in Figure 13(a).

2. A preliminary transfer from a candidate resonant orbit to the target variables is generated with the Q-law algorithm. As a result, the state and control history for this transfer is constructed, where the position history is represented as the purple arc in Figure 13(a).

3. Since Q-law fails to target the true anomaly, the location at the end of the preliminary transfer (red circle in Figure 13(a)) does not coincide with the anticipated final state. This discrepancy in positions is accommodated by shifting the yellow circle closer to the red circle by selecting a different final epoch. This new final epoch is determined via the equation,

$$JD_{f,new} = \underset{JD_f}{\arg\min} \, |\bar{r}_{Qf} - \bar{r}_f(JD_f)| \tag{5}$$

   Here, $\bar{r}$ denotes a position vector of the s/c with respect to Mars in the Mars-centered inertial frame, $\bar{r}_{Mars-s/c}$, following Equation (3), but represented as $\bar{r}$ for simplicity. The subscripts $f$ and $Qf$ correspond to the final state along the manifold to be targeted (yellow circle in Figure 13(a)) and the final location along the preliminary transfer generated with the Q-law strategy (red circle in Figure 13(a)), respectively. Note that $\bar{r}_f$ depends on the final epoch, $JD_f$, since the epoch determines the location of Phobos as well as the location along the manifold in the Mars-centered inertial frame. On the contrary, $\bar{r}_{Qf}$ is constant over different epochs, which is a valid assumption since the osculating orbital elements of Phobos around Mars do not change substantially. Then, Eq. (5) is equivalent to determining a new final epoch that minimizes the distance between the final state at the final epoch, $\bar{r}_f(JD_f)$, represented as the yellow circle, and the final location (the red circle) along the original trajectory generated with Q-law, $\bar{r}_{Qf}$, represented as the red circle.

4. The difference between the estimated and the new final epoch is defined as $\Delta JD_f = JD_{f,new} - JD_{f,est}$. An intermediate Mars-centered conic arc, with a period equal to $\Delta JD_f$, is introduced. Then, the semi-major axis corresponding to this period is computed as $a_{inter} = (Gm_{Mars}\Delta JD_f^2)^{1/3}$, where $Gm_{Mars} = 4.282 \times 10^4 km^3/s^2$ is the gravitational parameter of Mars. One revolution of this intermediate conic, i.e., the blue arc in Figure 13(a), is inserted into the state history of the state generated by Q-law. As the s/c spends more time on this conic, the distance between $\bar{r}_{Qf}$ and $\bar{r}_f$ is minimized.

5. The state and control histories, including the intermediate ballistic conic, is discretized to form an initial guess for the direct collocation scheme, as illustrated in Figure 13(b). Subsequently, the initial guess is computed for a feasible solution where the trajectory is continuous

along all segments while satisfying the boundary conditions. The feasible solution is then optimized for propellant consumption. An example of an optimized solution is plotted in Figure 14(b).

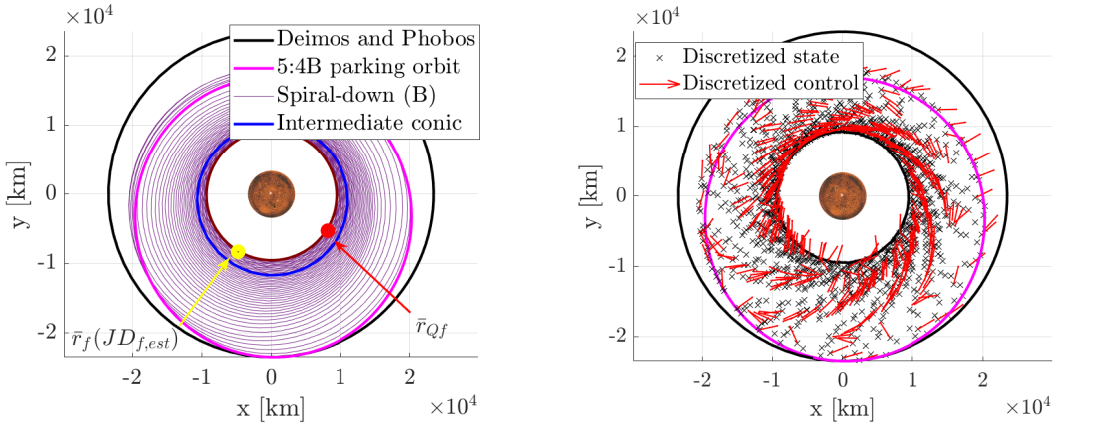


(a) Preliminary transfer generated with Q-law

(b) Discretized state and control for direct collocation

**Figure 13. Interfacing Q-law and direct collocation for generating spiral-down (B)**

The above steps comprise the interface between the Q-law control and the direct collocation targeter, and succeed in acquiring optimized transfers from each resonant orbit to the Phobos science orbit. The associated costs are included in Table 3. Note that $\Delta V$ corresponds to the equivalent $\Delta V$ computed as $\Delta V = I_{sp} g_0 \log\left(m_0/(m_0 - \Delta m)\right)$.

**Table 3. Low-Thrust Results: Q-law + direct collocation (*: optimized)**

| Candidate Orbits | | Spiral-down (A) | | | Spiral-down (B) | | | (A) + (B) | | |
|---|---|---|---|---|---|---|---|---|---|---|
| | | $\Delta m$ [kg] | $\Delta V$ $[m/s]$ | TOF [days] | $\Delta m$ [kg] | $\Delta V$ $[m/s]$ | TOF [days] | $\Delta m$ [kg] | $\Delta V$ $[m/s]$ | TOF [days] |
| Case 1 | 3:2 | 6.06 | 1217 | 34.37 | 4.58* | 954* | 30.67 | 10.63 | 2171 | 65.03 |
| | 3:4 | 4.69 | 938 | 26.62 | 9.38 | 1969 | 53.67 | 14.07 | 2907 | 80.29 |
| | 3:4 | 4.79 | 961 | 27.19 | 10.21 | 2157 | 58.43 | 15.00 | 3118 | 85.62 |
| | 5:4 | 5.49 | 1101 | 31.17 | 3.44* | 711* | 26.76 | 8.93 | 1813 | 57.93 |
| Case 2 | 3:2 | 6.00 | 1205 | 34.07 | 3.62* | 752* | 25.98 | 9.63 | 1957 | 60.06 |
| | 2:1 | 7.10 | 1430 | 40.29 | 4.58* | 961* | 31.50 | 11.68 | 2391 | 71.79 |
| | 2:1 | 7.10 | 1431 | 40.31 | 4.43* | 928* | 31.46 | 11.53 | 2359 | 71.77 |
| | 5:4 | 5.47 | 1096 | 31.02 | 3.35* | 693* | 25.48 | 8.82 | 1789 | 56.49 |

## CONCLUDING REMARKS

This investigation proposes a trajectory design strategy for observation of both Deimos and Phobos within the context of the CR3BP. Firstly, it is demonstrated that resonant orbits computed in the Mars-Deimos CR3BP model offer long term stability in a higher-fidelity ephemeris model, generally desirable to meet scientific requirements. Thus, such resonant trajectories are a good resource for periodic observation of Deimos, given that a s/c in this orbit repeatedly encounters around the moon. Additionally, it is demonstrated that by employing the MMAT method, it is possible to deduce trajectories departing Deimos that yield a connection to transfer to the vicinity of Phobos. In the context of this application, resonant orbits are promising candidates that grant access to Phobos, given their observational flybys of both moons but at the expense of a low $\Delta V$. As a result, an assessment of various resonant orbits is accomplished seeking access to CR3BP periodic orbits in

the vicinity of $L_2$ of the Mars-Phobos system. Using MMAT, a relationship is established between the variation of $JC_{MD}$ along a resonant orbit family and the cost to access Phobos. It is observed that the resonant orbit in its family with a higher value of $JC_{MD}$, the lower the cost to access the vicinity of Phobos. Once the resonant orbits that guarantee lower $\Delta V$s for impulsive transfers are identified, a Q-law strategy is interfaced in a scheme to transition the results to the low-thrust model and, thus, construct transfers from the resonant orbit towards the Phobos vicinity using low-thrust. The low-thrust algorithm addresses the fact that Q-Law does not target the true anomaly for the arrival at Phobos by adding an intermediate conic. This modification not only aids convergence in a higher-fidelity ephemeris model, but also results in an optimized transfer. As a result of the analysis, the $5:4$B resonant orbit serves as a suitable candidate for access from outside the Martian system; this orbit also offers frequent access to Deimos and more efficient access to Phobos compared to the other resonant orbits. To the extent that impulsive analysis is concerned, the resulting transfer (Figure 10(b)) is obtained in the patched 2BP-CR3BP model and then, using this transfer as an initial guess, it is transitioned to a higher-fidelity ephemeris model (Figure 14). The optimal low-thrust trajectory that connects the $5:4$B resonant orbit with the Phobos vicinity is also illustrated in Figure 14. It is noted that, given the small mass of Phobos, the $JC_{MP}$ variation to ensure capture around the moon is sufficiently small that the same transfer from a resonant orbit is applicable for capture into different orbits in the Phobos vicinity: both planar and spatial periodic orbits around $L_2$, or a quasi-satellite orbit around the moon. This generalization is applicable due to the low $\Delta V$ required to target instant 4 (defined in Figure 8) in the impulsive analysis: less than $10\ m/s$ is required to transfer from the arrival arc to the selected Lyapunov orbit in a higher-fidelity ephemeris model, reflected in Figure 14 (g). Further refinement of these trajectories can also incorporate the moon harmonics due to their irregular shapes, e.g., Phobos.

## ACKNOWLEDGEMENTS

The first three authors have equally contributed to the work. Assistance from colleagues in the Multi-Body Dynamics Research group at Purdue University is appreciated, as is the support from the Purdue University School of Aeronautics and Astronautics and College of Engineering, including access to the Rune and Barbara Eliasen Visualization Laboratory.

## REFERENCES

[1] R. Z. Sagdeev and A. V. Zakharov, "Brief History of the Phobos Mission," *Nature*, Vol. 341, No. 6243, 1989, pp. 581–585, 10.1038/341581a0.

[2] A. N. Deutsch, J. W. Head, K. R. Ramsley, C. M. Pieters, R. W. Potter, A. M. Palumbo, M. S. Bramble, J. P. Cassanelli, E. R. Jawin, L. M. Jozwiak, H. H. Kaplan, C. F. Lynch, A. C. Pascuzzo, L. Qiao, and D. K. Weiss, "Science Exploration Architecture for Phobos and Deimos: The Role of Phobos and Deimos in the Future Exploration of Mars," *Advances in Space Research*, Vol. 62, No. 8, 2018, pp. 2174 – 2186.

[3] S. L. Murchie, D. T. Britt, and C. M. Pieters, "The Value of Phobos Sample Return," *Planetary and Space Science*, Vol. 102, No. C, 2014, pp. 176–182, 10.1016/j.pss.2014.04.014.

[4] D. Koschny, H. Svedhem, and D. Rebuffat, "Phootprint - A Phobos Sample Return Mission Study," *40th COSPAR Scientific Assembly*, Vol. 40, Jan. 2014.

[5] T. H. Prettyman, S. Diniega, and C. A. Raymond, "PANDORA - Unlocking the Mysteries of the Moons of Mars," *AAS/Division for Planetary Sciences Meeting Abstracts #46*, AAS/Division for Planetary Sciences Meeting Abstracts, Nov. 2014.

[6] P. Lee, M. Benna, and D. Britt, "PADME (Phobos and Deimos and Mars Environment): A Proposed NASA Discovery Mission to Investigate the Two Moons of Mars.," *46th Lunar and Planetary conference*, 2015.

[7] M. Fujimoto, H. Miyamoto, K. Kuramoto, and t. MMX Science Board members, "JAXA's Martian Moons eXplortaion, MMX," *European Planetary Science Congress*, 2017.

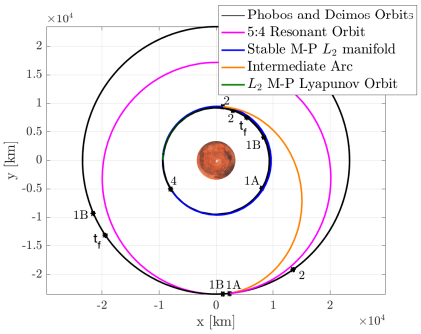


(a) Mars centered inertial frame (MARSIAU)

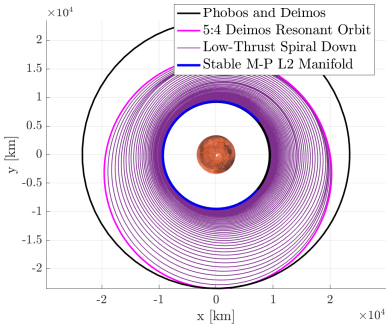


(b) Mars centered inertial frame (MARSIAU)

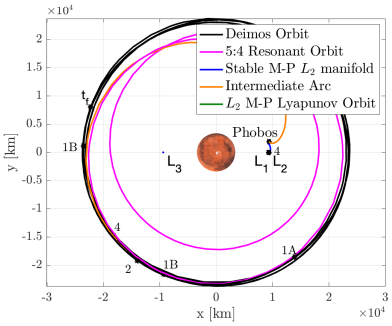


(c) Mars-Phobos rotating frame

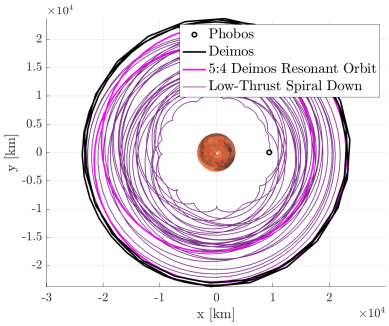


(d) Mars-Phobos rotating frame

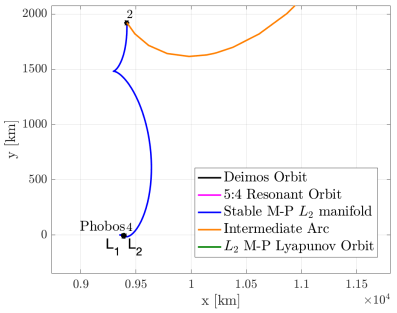


(e) Mars-Phobos rotating frame: zoomed in

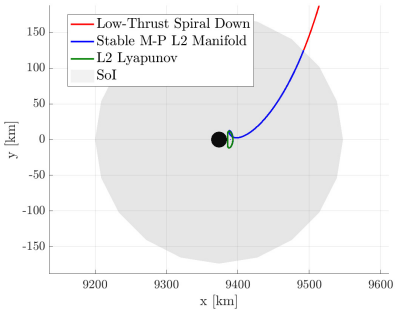


(f) Mars-Phobos rotating frame: zoomed in

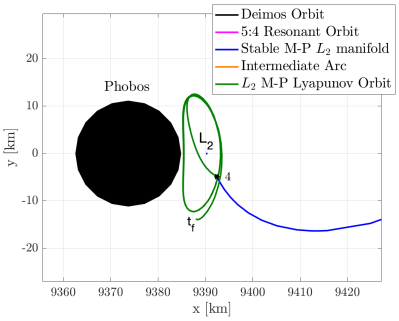


(g) Mars-Phobos rotating frame: zoomed in 2

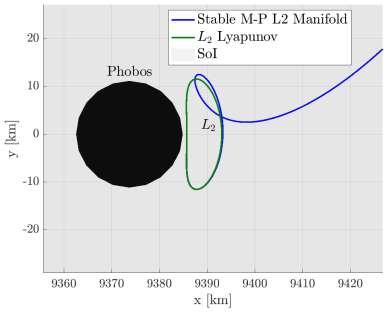


(h) Mars-Phobos rotating frame: zoomed in 2

**Figure 14. Transfers from 5 : 4B resonant orbit in the Sun-Mars-Phobos-Deimos ephemeris model: impulsive (left), low-thrust (right). Model: higher-fidelity ephemeris model. Epoch: 11/12/2020 22:00:00. For the impulsive engine,** $\Delta V = 643.9 m/s$, $TOF = 1.82$ **days and for the low-thrust engine,** $\Delta m = 3.35 kg$, $\Delta V = 692.9 m/s$, $TOF = 25.48$ **days**

.

[8] N. Bosanac, A. Diaz Artiles, V. Dang, F. Ebersohn, S. Gonzalez, J. Qi, N. Sweet, N. Tie, G. Valentino, A. Fraeman, A. Gibbings, T. Maddox, C. Nie, J. Rankin, T. Rebelo, and G. Taylor, "Manned Sample Return Mission to Phobos: A Technology Demonstration for Human Exploration of Mars," *IEEE Aerospace Conference Proceedings*, 03 2014, 10.1109/AERO.2014.6836251.
[9] S. Campagnola, C. H. Yam, Y. Tsuda, N. Ogawa, and Y. Kawakatsu, "Mission analysis for the Martian Moons Explorer (MMX) Mission," *Acta Astronautica*, Vol. 146, 03 2018.
[10] J. Englander, M. A. Vavrina, B. J. Naasz, R. G. Merrill, and M. Qu, "Mars, Phobos, and Deimos Sample Return Enabled by ARRM Alternative Trade Study Spacecraft," *AIAA/AAS Astrodynamics Specialist Conference*, 2014, 10.2514/6.2014-4354.
[11] N. Ogawa, Y. Tsuda, Y. Takei, H. Inoue, S. Takahashi, and Y. Kawakatsu, "Orbit Design for the Martian Moons Exploration Mission," *Transactions of the Japan Society for Aeronautical and Space Sciences, Aerospace Technology Japan*, Vol. 17, No. 3, 2019, pp. 398–403, 10.2322/tastj.17.398.
[12] A. Simonov, V. Pol, and A. Vorobyev, "Development of a Flight Scheme for a Perspective Spacecraft for Mars and its Satellites Exploration," *AIP Conference Proceedings*, Vol. 2171, 11 2019, p. 060004.
[13] A. L. Genova, D. Korsmeyer, M. Loucks, F. Y. Yang, and P. Lee, "Trajectory Design for the Phobos and Deimos Mars Environment Spacecraft," *AIAA/AAS Astrodynamics Specialist Conference*, 2016.
[14] E. Canalias, L. Lorda, and J. Laurent-Varin, "Design of Realistic Trajectories for the Exploration of Phobos," *Space Flight Mechanics Meeting, 2018*, No. 210009, 2018, 10.2514/6.2018-0716.
[15] H. Chen, E. Canalias, D. Hestroffer, and X. Hou, "Stability Analysis of Three-Dimensional Quasi-Satellite Orbits around Phobos," *Proceedings of the International Astronautical Congress, IAC*, 2018.
[16] M. S. Wallace, J. S. Parker, N. J. Strange, and D. Grebow, "Orbital Operations for Phobos and Deimos Exploration," *AIAA/AAS Astrodynamics Specialist Conference 2012*, 2012, pp. 1–10.
[17] M. Zamaro and J. D. Biggs, "Natural Motion around the Martian Moon Phobos: the Dynamical Substitutes of the Libration Point Orbits in an Elliptic Three-Body Problem with Gravity Harmonics," *Celestial Mechanics and Dynamical Astronomy*, Vol. 122, No. 3, 2015, pp. 263–302.
[18] Y. Wang and X. Wu, "Analysis of Phobos' Dynamical Environment Considering Effects of Ephemerides and Physical Libration," *Monthly Notices of the Royal Astronomical Society*, Vol. 497, 2020, pp. 416–434, 10.1093/mnras/staa1948.
[19] E. Fantino and R. Castelli, "Efficient Design of Direct Low-Energy Transfers in Multi-Moon Systems," *Celestial Mechanics and Dynamical Astronomy*, Vol. 127, 10 2016, 10.1007/s10569-016-9733-9.
[20] C. R. Short, D. Blazevski, K. C. Howell, and G. Haller, "Stretching in Phase Space and Applications in General Nonautonomous Multi-Body Problems," *Celestial Mechanics and Dynamical Astronomy*, Vol. 122, No. 3, 2015, pp. 213–238, 10.1007/s10569-015-9617-4.
[21] D. Canales, K. Howell, and E. Fantino, "Moon-to-Moon Transfer Methodology for Multi-Moon Systems in the Coupled Spatial Circular Restricted Three-Body Problem," *AAS/AIAA Astrodynamics Specialist Conference*, 08 2020.
[22] G. Lantoine, R. P. Russell, and S. Campagnola, "Optimization of Low-Energy Resonant Hopping Transfers between Planetary Moons," *Acta Astronautica*, Vol. 68, No. 7, 2011, pp. 1361 – 1378.
[23] S. Campagnola, P. Skerritt, and R. P. Russell, "Flybys in the Planar, Circular, Restricted, Three-Body Problem," *Celestial Mechanics and Dynamical Astronomy*, Vol. 113, No. 3, 2012, pp. 343–368.
[24] A. L. Genova, D. Korsmeyer, L. Plice, M. Loucks, and F. Y. Yang, "Trajectory Design for the Phobos and Deimos Mars Environment (PADME) Spacecraft," *AIAA/AAS Astrodynamics Specialist Conference, 2016*, 2016.
[25] C. Acton, N. Bachman, B. Semenov, and E. Wright, "A Look Toward the Future in the Handling of Space Science Mission Geometry," *Planetary and Space Science*, 2017.
[26] R. Woolley and Z. Olikara, "Optimized Low-Thrust Missions from GTO to Mars," *IEEE Aerospace Conference Proceedings*, Vol. 2019-March, 2019, 10.1109/AERO.2019.8741558.
[27] R. C. Woolley, F. Laipert, A. K. Nicholas, and Z. Olikara, "Low-thrust Trajectory Bacon Plots for Mars Mission Design," *Advances in the Astronautical Sciences*, Vol. 168, 2019, pp. 2833–2846.
[28] G. Mingotti, F. Topputo, and F. Bernelli-Zazzera, "Earth-Mars Transfers with Ballistic Escape and Low-Thrust Capture," *Celestial Mechanics and Dynamical Astronomy*, Vol. 110, No. 2, 2011, pp. 169–188.
[29] D. J. Dichmann, R. Lebois, and J. P. Carrico, "Dynamics of Orbits Near 3:1 Resonance in the Earth-Moon System," *The Journal of the Astronautical Sciences*, Vol. 60, No. 1, 2013, pp. 51–86.
[30] D. J. Dichmann, J. J. Parker, T. W. Williams, and C. R. Mendelsohn, "Trajectory Design for the Transiting Exoplanet Survey Satellite," *International Symposium on Space Flight Dynamics*, 2014.
[31] M. Vaquero, "Poincaré Sections and Resonant Orbits in the Restricted Three-Body Problem," M.S. Thesis, Purdue University, West Lafayette, Indiana, 2010.
[32] A. E. Petropoulos, "Low-Thrust Orbit Transfers Using Candidate Lyapunov Functions with a Mechanism for Coasting," *AIAA/AAS Astrodynamics Specialist Conference*, 2004.
[33] R. Pritchett, *Strategies for Low-Thrust Transfer Design Based on Direct Collocation Techniques*. Ph.D. Dissertation, Purdue University, West Lafayette, Indiana, 08 2020.
[34] G. Huntington, D. Benson, and A. Rao, "A Comparison of Accuracy and Computational Efficiency of Three Pseudospectral Methods," *Collection of Technical Papers - AIAA Guidance, Navigation, and Control Conference 2007*, Vol. 1, 08 2007, 10.2514/6.2007-6405.